Original Paper

Pole Segmentation Shaped by Sinusoidal, Trapezoidal, and Harmonic Injection PWM for Torque Ripple Reduction in Permanent Magnet Synchronous Machines

Khristian M. de Andrade Jr.◉[1],[*], Bernardo P. de Alvarenga◉[*], Geyverson T. de Paula◉[*]

[1]Federal University of Goiás, School of Electrical, Mechanical and Computer Engineering, Goiânia, 74605-010, Brazil.

e-mail: khristian@discente.ufg.br[*]; bernardo_alvarenga@ufg.br; geyverson@ufg.br.
[*]Corresponding author.

ABSTRACT The present paper proposes three methods to reduce the torque ripple in Permanent Magnet Synchronous machine by decreasing the cogging torque peak and back-EMF harmonic content. These methods consider the pole segmentation technique, but the distribution and width of the segments are determined by PWM techniques. Sinusoidal, trapezoidal and harmonic injection PWM are assigned to Methods 1, 2 and 3 in that order. This methods can decrease the cogging torque peak and also improve the harmonic content of the back-EMF, thus reducing the torque ripple. Furthermore, the methods were validated by means of a finite elements analysis. Method 3 achieved the best results for both 4- and 8-pole machines, reducing the cogging torque peak by up to 79.53% and increasing the average torque by 6.43%. It also reduced the magnet volume in the 4-pole machine.

KEYWORDS pole segmentation, PWM techniques, permanent magnet synchronous machine, torque ripple reduction.

I. INTRODUCTION

The increase in the demand for electric traction and wind energy, along with the discovery/development of new permanent magnets has attracted more attention to the permanent magnet synchronous machine (PMSM) recently. This machine presents some advantages over the induction motors, such as higher power density, easier control and low maintenance [1], [2]. However, the presence of the magnets causes a characteristic ripple in the output torque, known as the cogging torque. The cogging torque is due to the tendency of alignment between magnets edges and slot openings. Since the torque ripple causes mechanical stresses, its mitigation is object of numerous researches around the world.

Two main approaches are commonly found in the literature for reducing cogging torque during the early design stage. The first involves modifying the geometry of the stator through techniques such as unequal teeth [3], [4], dummy slots [4], [5], or skewing the stator laminations [6]. Although these methods can be effective, they introduce several trade-offs. Unequal teeth and dummy slots can reduce mechanical strength and increase magnetic losses or leakage. They can also lead to magnetic anisotropies and localized saturation – narrow teeth tend to saturate more easily. Skewing the stator laminations, also presents drawbacks: it reduces average torque and back-EMF amplitude, increases magnetic leakage, and often requires a longer axial core to preserve the active length. Furthermore, skewing complicates manufacturing and assembly, increases production costs, and makes it more difficult to implement and align cooling channels and structural supports that can negatively impact thermal performance and mechanical integrity.

The second approach focuses on modifying the rotor or magnet geometry, such as adjusting the pole arc to pole pitch ratio [4], [7], pole shifting [7], skewing the magnets [8], optimizing the magnets shape [9]–[12], or, as proposed in this paper, applying pole segmentation [13]–[17]. Optimizing the pole arc ratio can effectively reduce cogging torque but may lower average torque and back-electromotive force (back-EMF), increase sensitivity to manufacturing tolerances, and introduce higher-order harmonics. Pole shifting may lead to unbalanced magnetic forces, increased vibrations, and requires careful tuning for each configuration. Skewing the magnets reduces torque and back-EMF amplitude due to flux spreading and complicates precise alignment. Optimized magnet shapes require computationally intensive design and are difficult to fabricate accurately, with potential issues like misalignment, mechanical fragility, and demagnetization under stress. These methods, while effective, often involve trade-offs that must be carefully balanced during design.

The pole segmentation technique involves dividing each rotor pole into smaller segments. The main distinction among prior works [13]–[17] lies in how the number, width, and

spacing of these segments are defined. In [16] and [17], these parameters are derived using PWM-based approaches. In [16], they are determined by solving a non-linear system of equations aimed at eliminating specific harmonics from the airgap flux density. A key drawback of this method is the growing complexity of the non-linear system as more harmonics are targeted. In contrast, [17] determines the segment distribution by comparing the desired airgap permeance waveform to a triangular reference, simplifying the design process. Although effective in reducing the cogging torque peak, this technique can also diminish the overall magnetic flux, resulting in lower average torque and back-EMF.

The novelty of the present work is the PWM techniques considered for the pole segmentation of the PMSM. These techniques are referred here as Sinusoidal (Method 1), Trapezoidal (Method 2) and Harmonic Injection (Method 3) PWM and will be described further. Their output pulse sequence is obtained by a comparison between the desired airgap flux density waveform (the modulating wave), and a triangular one (the carrier). The advantages of the proposed methods over [16] and [17] are the obtaining of an airgap flux density waveform similar to the modulating waveform, the elimination of almost every lower order harmonics and easier/similar computational implementation. In addition, Methods 2 and 3 help mitigate the magnetic flux reduction inherent to the pole segmentation technique.

This paper is divided into three sections. In Section II a simple mathematical model for the cogging torque is developed and described. Section III describes the PWM techniques considered and the proposed methods. The results obtained with a finite elements analysis and the discussions are presented in Section IV. Finally, conclusions are drawn and references presented.

II. COGGING TORQUE MATHEMATICAL MODELING

This section presents the modeling of the cogging torque considered in the research. As stated above, the cogging torque arises from the tendency of alignment between magnets edges and slot openings. It is possible to model this phenomenon from the machine magnetic energy when no current flows through the windings.

Some simplifications can be made to reduce the complexity of the cogging torque model. First, the variation of the machine energy is considered equal to the variation of the airgap energy. Second, the effects of fringing, leakage and saturation are neglected.

The airgap energy W can be obtained from the integration of the airgap energy density in its volume V, as shown in (1) [13], [14].

$$W = \int_V \frac{B_g^2}{2\mu_0} dV \tag{1}$$

where $B_g^2/2\mu_0$ is the airgap energy density, B_g is the airgap flux density and μ_0 is the free space permeability.

Now, assuming that the value of the flux density in the middle of the airgap is B, the integral in (1) can be expanded using polar coordinates, resulting in (2).

$$W(\alpha) = \frac{\pi L_s}{4\mu_0} \left(R_s^2 - R_m^2 \right) \int_0^{2\pi} B^2(\theta, \alpha)\, d\theta \tag{2}$$

in which L_s is the rotor stack length, R_s is the radius over the slots, R_m is the outer radius of the magnets, θ is the airgap angle and α the rotor angle.

The airgap flux density B of a slotted machine can be rewritten in terms of a modulating waveform and the airgap flux of a slotless machine B_s. This modulating waveform is referred as the airgap permeance function λ and models the effects of the slots openings. In the ideal case, λ is assumed to be equal to one under the stator teeth and zero under the slots, resulting in a perfect square-shaped waveform. This way, (2) now becomes (3).

$$W(\alpha) = \frac{\pi L_s}{4\mu_0} \left(R_s^2 - R_m^2 \right) \int_0^{2\pi} \lambda^2(\theta)\, B_s^2(\theta, \alpha)\, d\theta \tag{3}$$

Now, the cogging torque can be obtained via (4).

$$T_C(\alpha) = -\frac{\partial W(\alpha)}{\partial \alpha} \tag{4}$$

It is possible to solve the integral in (3) using the Fourier series of λ^2 and B_s^2, as shown in (5).

$$\begin{aligned} \lambda^2 &= \lambda_0 + \sum_{m=1}^{\infty} \lambda_{mS} \cos(mS\theta) \\ B_s^2 &= B_0 + \sum_{n=1}^{\infty} B_{n2p} \cos[n2p(\theta - \alpha)] \end{aligned} \tag{5}$$

where m and n are positive integers, λ_{mS} and B_{n2p} are the Fourier coefficients of the airgap permeance and slotless flux density, respectively. Also, S is the number of slots and $2p$ the number of poles.

Theoretical waveforms in Fig. 1, obtained under ideal assumptions, illustrate the behavior of λ^2, B_s^2, and their harmonics. B_m represents an arbitrary air-gap flux density level. As the waveforms deviate from an ideal 50% duty-cycle square wave, their asymmetry gives rise to both even and odd harmonics.

Substituting (5) in (3) and then in (4) and using orthogonality properties results in (6) [13], [14]. N_L is the least common multiple of $2p$ and S and k is a positive integer.

$$T_C(\alpha) = \frac{\pi L_s}{4\mu_0} \left(R_s^2 - R_m^2 \right) \sum_{k=1}^{\infty} k N_L \lambda_{kN_L} B_{kN_L} \sin(kN_L\alpha) \tag{6}$$

The cited methods for reducing the cogging torque can be derived from (6). The techniques focused on the stator change the coefficients λ_{kN_L}, whereas those focused on the rotor, change the B_{nN_L}. Fig. 1 shows that λ_{kN_L} amplitude decreases with order, so larger N_L results in lower cogging torque.

III. PROPOSED METHODS

In this sections the proposed methods are described in detail as well as the PWM techniques associated to them.
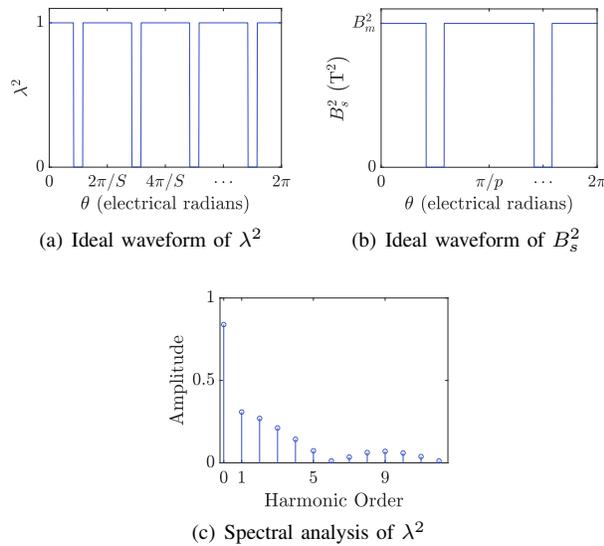
(a) Ideal waveform of λ^2

(b) Ideal waveform of B_s^2

(c) Spectral analysis of λ^2

FIGURE 1. Analysis of the ideal waveforms of λ^2 and B_s^2.

As mentioned, the methods combine the pole segmentation (distribution and width of the segments) to the output pulse sequence of PWM techniques.

A. METHOD 1: SINUSOIDAL PWM

In Method 1, the distribution and width of the pole segments are determined by means of the sinusoidal PWM technique. This technique employs two sinusoidal waves, one is the negative of the other, as the modulating ones and a triangular waveform as the carrier. For each modulating waveform, a square pulse sequence is attributed. A positive pulse is generated wherever the instantaneous value of the carrier is smaller then the modulating ones, otherwise, a negative pulse is generated. The output sequence is the difference between the two pulse sequences.

Once the output sequence is obtained, the pole can be shaped. To each positive pulse, a north pole magnet is assigned with the same position and width of the pulse. South pole magnets are assigned to negative pulses. Fig. 2 illustrates the described process.

In Figs. 2, 3 and 4, A_m, A_c, A and A_f are the amplitude of the modulating waveform, carrier, pulse sequence and fundamental, respectively, and m_f is the frequency modulating index, defined in (7). These amplitudes are chosen arbitrarily and do not need to match the actual desired airgap flux density values; they are selected solely to define the pole shape and predict the resulting harmonic content of the airgap flux density.

$$m_f = \frac{f_c}{f_m} = \frac{2\pi f_c}{p} \tag{7}$$

where f_m is the modulating fundamental frequency, assumed here as equal to the fundamental frequency of the airgap flux density and f_c the frequency of the carrier.

In addition, the harmonic content of the pulse sequence can also be seen in Fig. 2. Note that this PWM technique

eliminates all harmonics, except those in regions near the multiples of $2m_f$. This characteristic extends to the airgap flux density, as will be shown later.
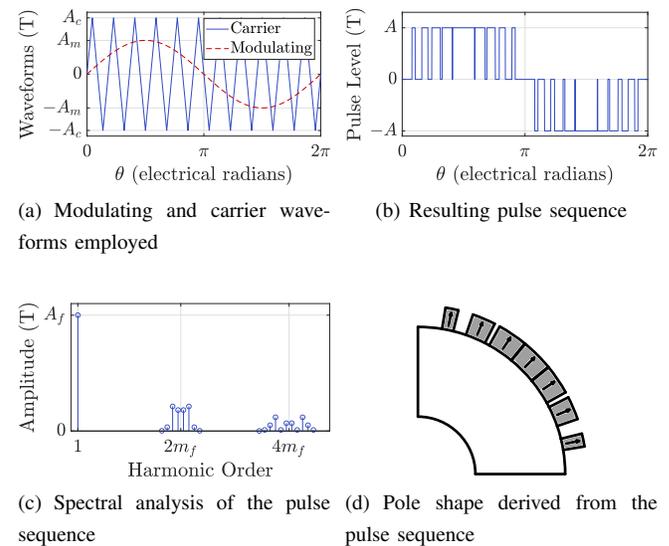

(a) Modulating and carrier waveforms employed

(b) Resulting pulse sequence

(c) Spectral analysis of the pulse sequence

(d) Pole shape derived from the pulse sequence

FIGURE 2. Method 1 – Sinusoidal PWM-based pole segmentation.

B. METHOD 2: TRAPEZOIDAL PWM

Method 2 is similar to Method 1, the difference is the employed PWM technique. Here, the two modulating waveforms are trapezoidal. Fig. 3 illustrates the output sequence, its harmonic content and the pole shaping. Note that this technique increases the fundamental amplitude at the cost of the presence of low order harmonics.
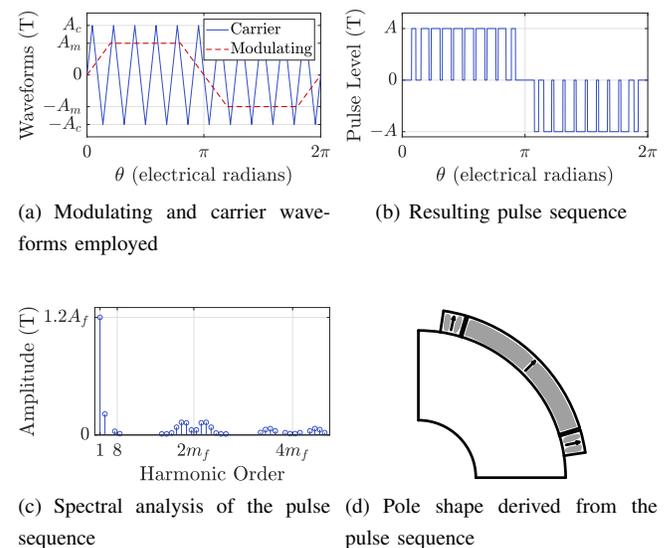

(a) Modulating and carrier waveforms employed

(b) Resulting pulse sequence

(c) Spectral analysis of the pulse sequence

(d) Pole shape derived from the pulse sequence

FIGURE 3. Method 2 – Trapezoidal PWM-based pole segmentation.

Eletrônica de Potência, Rio de Janeiro, v. 30, e202551, 2025.

3

C. METHOD 3: HARMONIC INJECTION PWM

The third method closely resembles the previous two approaches. To determine the optimal value of the third-harmonic injection coefficient a, consider the function F defined in (8). The objective is to enhance the amplitude of the fundamental component of F by minimizing its peak value through an appropriate choice of a.

To this end, one must first differentiate (8) with respect to θ, set the derivative to zero, and solve for the angle that maximizes F as a function of a. This yields an expression for the peak value of F in terms of a. The peak expression is differentiated with respect to a, and solving the result yields the optimal value $a = 1/6$ [18].

$$F = K\,A_c\,[\sin{(p\theta)} + a\sin{(3p\theta)}] \tag{8}$$

With a set, F peaks at $0.866, K, A_c$; choosing $K = 1.15$ raises the fundamental amplitude by about 15.5%.

The resulting modulating waveform, F_m, is given in (9), obtained by substituting $a = 1/6$ and $K = 1.15$ into (8). Figure 4 shows the resulting waveform, its frequency spectrum, and the corresponding pole geometry.

$$F_m = 1.15A_c\sin{(p\theta)} + 0.19A_c\sin{(3p\theta)} \tag{9}$$

(a) Modulating and carrier waveforms employed

(b) Resulting pulse sequence

(c) Spectral analysis of the pulse sequence

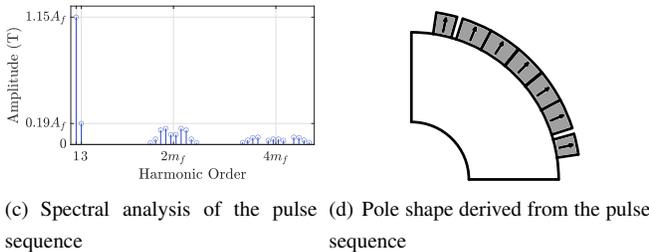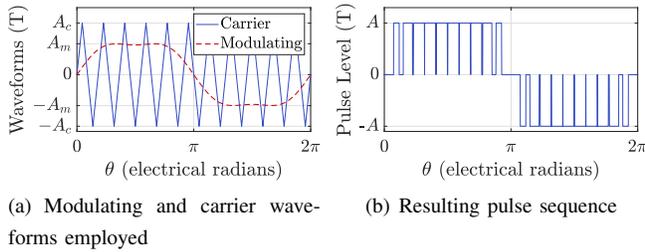(d) Pole shape derived from the pulse sequence

FIGURE 4. **Method 3 – Harmonic Injection PWM-based pole segmentation.**

D. TORQUE RIPPLE REDUCTION

As mentioned, the cogging torque is the main component of the PMSM torque ripple. However, the interaction between magnets, represented by the back-EMF, and the supplied current harmonics also contribute to the torque ripple. The proposed methods allow a reduction in the back-EMF harmonic content and also a reduction in the cogging torque peak, as will be described here. Consequently, the torque ripple mitigation is achieved with the proposed methods.

The airgap flux density waveform follows a pattern defined by the shape of the poles. This way, ideally, this waveform is equal to the output pulse sequence of the PWM techniques when the methods are applied to shape the poles. Therefore, the airgap flux density will have the same harmonic content of the respective PWM technique used to shape the magnets. In other words, the airgap flux density harmonics are shifted to regions around the multiples of $2m_f$.

Similarly to the airgap flux density harmonics, the ones of B_s^2 are also shifted, but to values near the multiples of m_f, as shown in Fig. 5. This fact can be used to reduce the cogging torque peak. In order to accomplish this reduction, the value of m_f must be chosen as to prevent any of the high amplitude harmonics of Fig. 5 to be an integer multiple of $N_L/2p$. Also, due to the behavior of λ_{kN_L}, m_f must be high, but not as high as to compromise the machine construction feasibility.
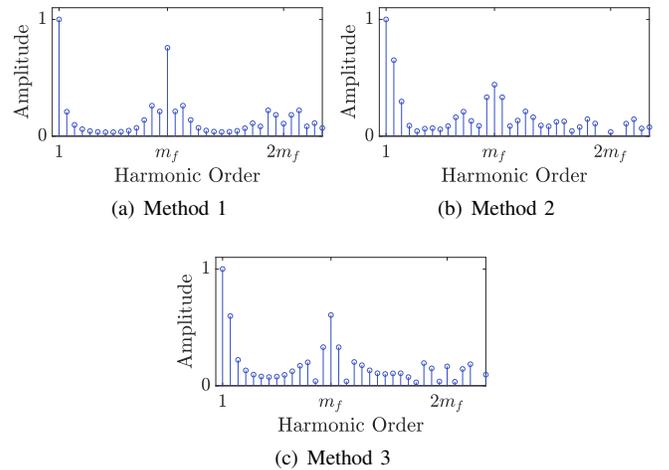

(a) Method 1

(b) Method 2

(c) Method 3

FIGURE 5. **Normalized Harmonic content of B_s^2 for all three methods.**
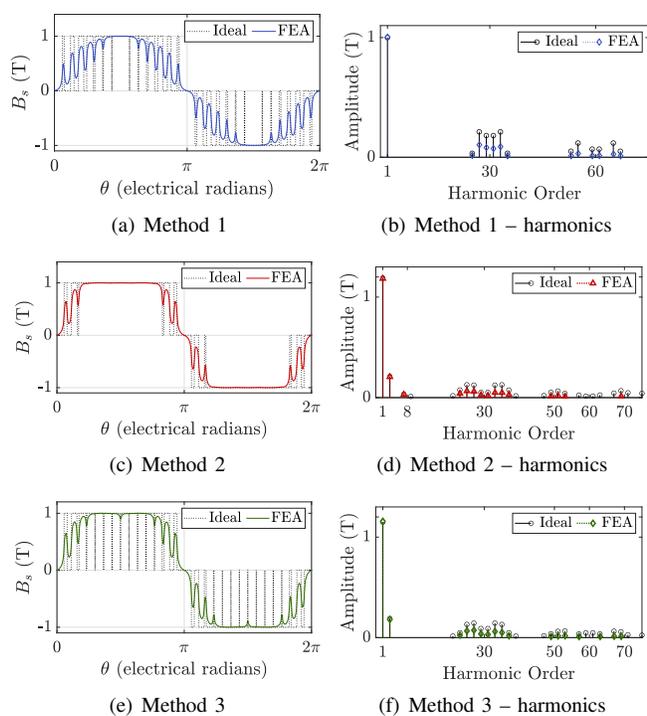
IV. RESULTS AND DISCUSSIONS

All three proposed methods were validated via finite element analysis (FEA), and the results are discussed herein. The methods were applied to surface-mounted permanent magnet machines with four and eight poles. Reference machines with non-segmented poles and optimized pole arc to pole pitch ratios following the guidelines reported in [4], [7] to minimize cogging torque were used for benchmarking. The main design parameters are summarized in Table 1.

The airgap flux density waveforms (ideal and FEA) and their spectral analysis for the 4-pole machine is presented in Fig. 6 for the three methods and $m_f = 15$. It can be seen that the ideal and FEA waveforms are very similar an close to each other, including their harmonic content. The difference in their shape and the attenuation in the amplitude of the high order harmonics are caused by the leakage and fringing effects that have been neglected in the formulation. Similar results were found for the 8-pole machine, thus they have been intentionally omitted.

A constraint has been added to the analysis considering the machine construction feasibility. Distances between seg-

TABLE 1. Machines Parameters

Parameter	Value		Unit
	4-pole	8-pole	
Rated Power	1	1	HP
Rated Speed	1500	1500	rpm
Stator Inner Diameter	96	96	mm
Stator Outer Diameter	182	132	mm
Stack Length	102	102	mm
Pole arc	75	30	°
Airgap	1	1	mm
Magnets Thickness	6	6	mm
Slot Openings	2	2	mm
Turns per Coil	19	7	-
Wire Gauge	20	16	AWG
Magnets Material	NdFeB 32 MGOe		-

(a) Method 1   (b) Method 1 – harmonics

(c) Method 2   (d) Method 2 – harmonics

(e) Method 3   (f) Method 3 – harmonics

FIGURE 6. Ideal and FEA airgap flux density waveforms for the 4-pole machine, $m_f = 15$ and their corresponding harmonics for all methods.

ments smaller than 0.2° (mechanical) have been discarded. This constraint had no significant impact on the 4-pole machine result, but for m_f values above 25 for the 8-pole machine, the airgap flux density starts to become distorted, as shown in Fig 7 for $m_f = 30$ and Method 1.

The back-EMF waveform is similar to the one of the airgap flux density, as shown in Fig. 8 for the 4-pole machine and $m_f = 15$. It can be seen that their waveforms is similar to the modulating waveforms considered for each method.

Air-gap flux density harmonic reduction is evident from the back-EMF total harmonic distortion (THD). From Fig. 9, it can be noted that the THD for Method 1 decreases as m_f

(a) Airgap flux density   (b) Spectral analysis
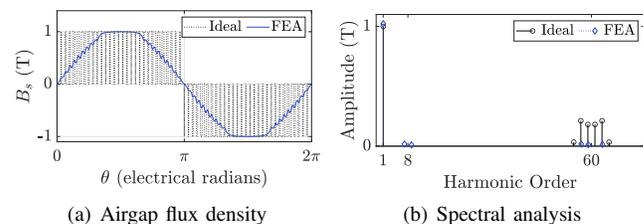
FIGURE 7. Distortion in the airgap flux density waveform and its harmonic content for the 8-pole machine using Method 1 with $m_f = 30$.

increases and is much smaller than that of Methods 2 and 3. Also, Methods 2 and 3 have an almost constant THD for different values of m_f due to the presence of low order harmonics in these methods.

In Fig. 5, the harmonics of B_s^2 for all methods are presented. Now, from Fig. 10, it is possible to notice that when those harmonic orders with the higher amplitudes are multiples of $N_L/2p$ a high peak cogging torque is noticed. The mentioned harmonics orders are of m_f, $m_f \pm 2$ and $m_f \pm 1$ for Method 1 and m_f, $m_f \pm 1$ and $m_f \pm 2$ for Methods 2 and 3 in descending order of amplitude.

The machines under study have 24 slots and either four or eight poles. Therefore, the harmonic orders m_f must not be multiples of six for the 4-pole machine, nor multiples of three for the 8-pole machine, since this represents the worst-case scenarios. Moreover, regardless of the m_f value, a harmonic multiple of three always occurs, causing higher cogging torque in the 8-pole machine than in the 4-pole machine. The observed reduction in cogging torque with increasing m_f is attributed to the behavior of the λ^2 harmonics.

Fig. 11 shows the average torque as a function of m_f for both machines and all methods. For the 4-pole machine, Methods 2 and 3 exhibit smaller attenuation ($\sim$3% and sim4%, respectively) compared with Method 1 ($\sim$17%). In the 8-pole machine, Method 1 produced an average torque $\sim$5% below the reference, whereas Methods 2 and 3 increased the average torque by $\sim$9% and $\sim$7%, respectively. These improvements result from the higher fundamental amplitude of the air-gap flux density achieved with Methods 2 and 3.

As previously discussed, cogging torque is the main source of torque ripple, calculated according to [19], as confirmed in Fig.12, which shows similar trends to Fig.10. For the 4-pole machine, Methods 1, 2, and 3 reduced the cogging torque peak by $\sim$59%, $\sim$67%, and $\sim$83%, resulting in torque ripple reductions of $\sim$51%, $\sim$64%, and $\sim$80%. In the 8-pole machine, the corresponding cogging torque peak reductions were $\sim$78%, $\sim$77%, and $\sim$79%, with torque ripple reduced by $\sim$76%, $\sim$78%, and $\sim$80%, respectively.

Some typical torque waveforms are shown in Fig. 13 for all methods and both machines, considering $m_f = 15$. It is possible to notice the variation in the average value. The presence of higher-order harmonics in the method waveforms is evident from their more oscillatory patterns.
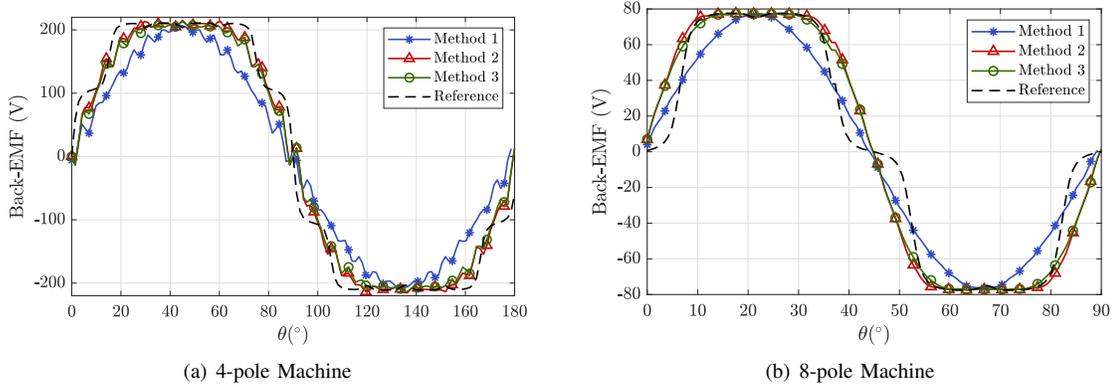
| (a) 4-pole Machine | (b) 8-pole Machine |

FIGURE 8. Back-EMF waveforms for the 4-pole and 8-pole machines with $m_f = 15$.

| (a) 4-pole Machine | (b) 8-pole Machine |
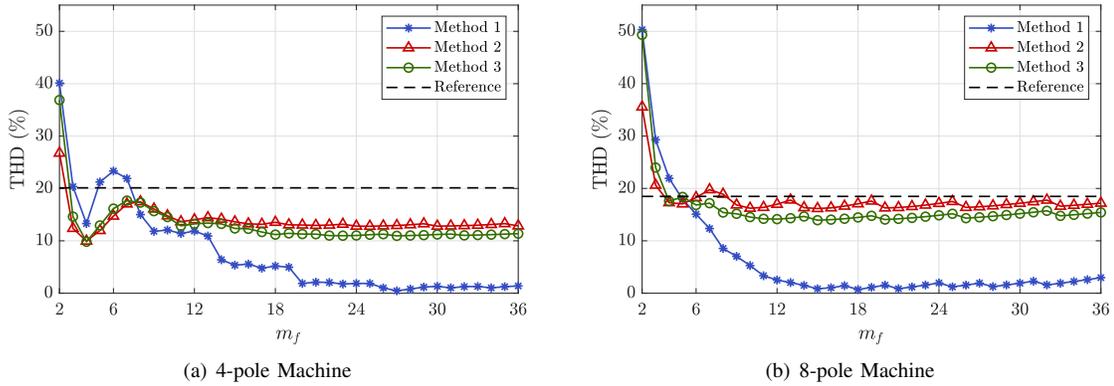
FIGURE 9. THD of the back-EMF as a function of m_f for all three methods in both machine configurations.
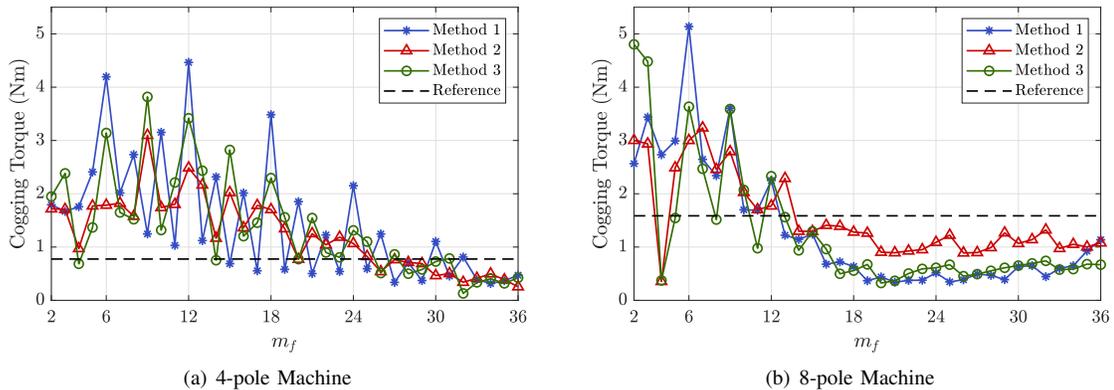

| (a) 4-pole Machine | (b) 8-pole Machine |

FIGURE 10. Cogging torque peak values for 4-pole and 8-pole machines as a function of m_f.

One advantage of segmenting the poles is the reduction in magnet volume, which directly lowers machine cost. Fig. 14 shows the total magnet volume for both machines as a function of m_f. For the 8-pole reference machine, the chosen magnet arc results in a volume 20.89% lower than that of the proposed methods; however, this machine also exhibits a lower average torque and higher cogging torque. A correlation between magnet volume and the air-gap flux density/average torque can thus be observed.

In summary, all methods effectively reduce the cogging torque peak, but each presents specific advantages and drawbacks. Method 1 yields the lowest back-EMF THD and magnet volume but suffers from the highest average torque attenuation. Method 2 minimizes torque attenuation, though at the expense of increased magnet volume and higher back-EMF THD. Method 3 provides the greatest cogging torque reduction and achieves torque attenuation and magnet volume similar to Method 2, while its back-EMF THD falls between those of Method 1 and Method 2.
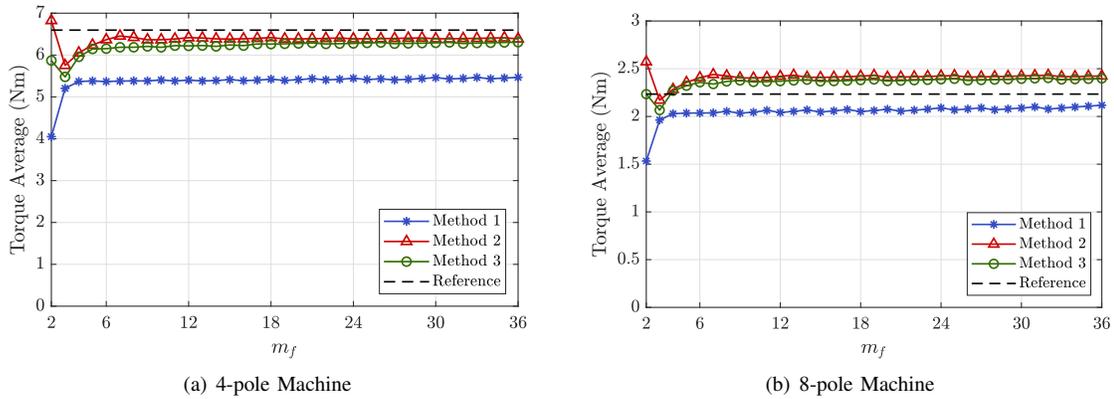
(a) 4-pole Machine

(b) 8-pole Machine

FIGURE 11. Average electromagnetic torque for both machines and all methods across varying m_f values.

(a) 4-pole Machine
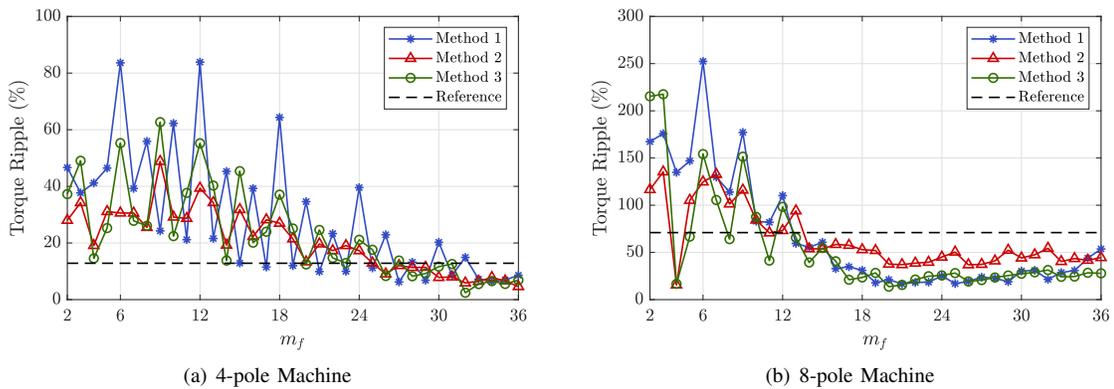
(b) 8-pole Machine

FIGURE 12. Torque ripple variation with m_f for the 4-pole and 8-pole machines under each proposed method.

(a) 4-pole Machine
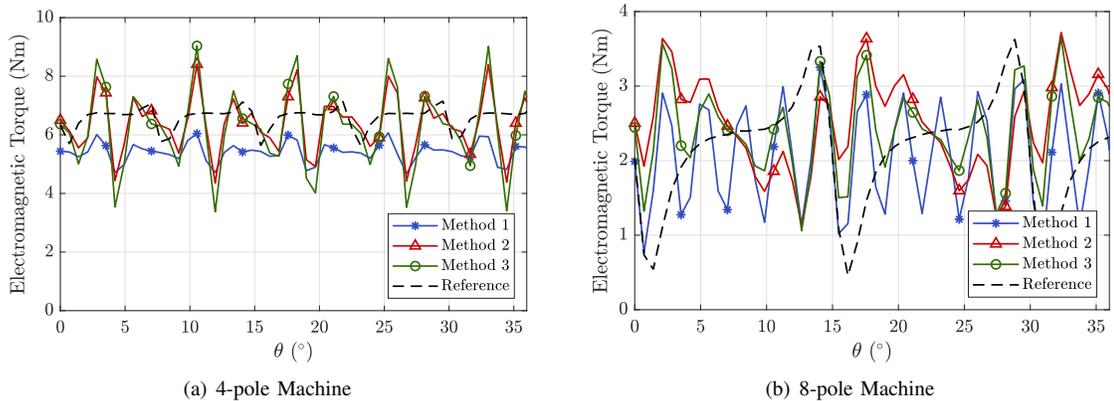
(b) 8-pole Machine

FIGURE 13. Representative electromagnetic torque waveforms for each method and machine type at $m_f = 15$.

V. CONCLUSION

The three proposed methods offer a new approach to mitigating torque ripple in PMSMs by combining pole segmentation with sinusoidal, trapezoidal, or harmonic injection PWM to define the segment distribution and width. Their main advantages are ease of implementation, low computational effort, and effective reduction of cogging torque and back-EMF harmonics. The main drawback is a decrease in average torque, an inherent effect of pole segmentation. Among the

methods, Method 3 achieved the best results for both 4-pole and 8-pole machines—particularly the latter reducing the cogging torque peak by up to 79.53% and increasing average torque by 6.43%. Finally, cogging torque, back-EMF, and torque remain strongly dependent on m_f; excessive values raise pole construction complexity and should therefore be avoided.
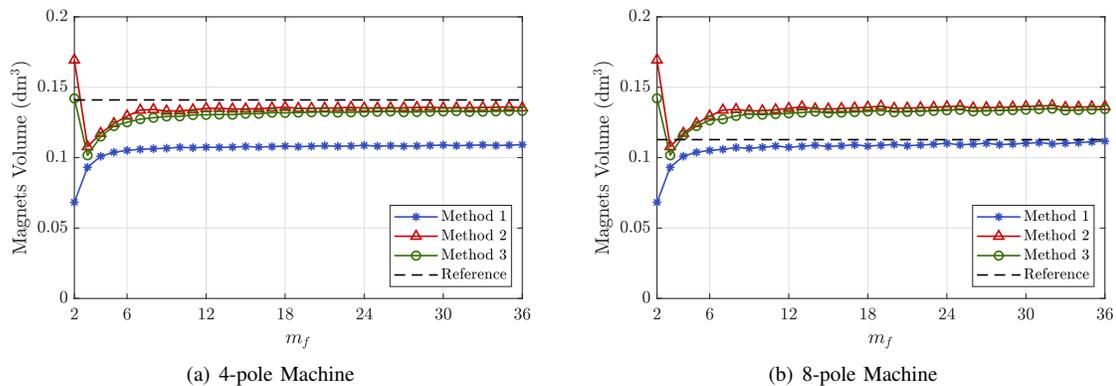
Eletrônica de Potência, Rio de Janeiro, v. 30, e202551, 2025.

7

(a) 4-pole Machine

(b) 8-pole Machine

FIGURE 14. Magnet volume required for both machines as a function of m_f.

ACKNOWLEDGMENT

AUTHOR'S CONTRIBUTIONS

K.M.ANDRADE JR: Data Curation, Formal Analysis, Writing – Original Draft. **B.P.ALVARENGA:** Supervision, Writing – Review & Editing. **G.T.PAULA:** Conceptualization, Formal Analysis, Supervision, Writing – Original Draft, Writing – Review & Editing.

PLAGIARISM POLICY

This article was submitted to the similarity system provided by Crossref and powered by iThenticate – Similarity Check.

DATA AVAILABILITY

The data used in this research is available in the body of the document.

REFERENCES

[1] E. Sulaiman, T. Kosaka, N. Matsui, "High Power Density Design of 6-Slot–8-Pole Hybrid Excitation Flux Switching Machine for Hybrid Electric Vehicles", *IEEE Transactions on Magnetics*, vol. 47, no. 10, pp. 4453–4456, 2011, doi:10.1109/TMAG.2011.2140315.

[2] J. R. Hendershot, T. J. E. Miller, *Design of Brushless Permanent-Magnet Motors*, Clarendon Press, 2023.

[3] J. Xintong, X. Jingwei, L. Yong, L. Yongping, "Theoretical and Simulation Analysis of Influences of Stator Tooth Width on Cogging Torque of BLDC Motors", *IEEE Transactions on Magnetics*, vol. 45, no. 10, pp. 4601–4604, 2009, doi:10.1109/TMAG.2009.2022639.

[4] S.-M. Hwang, J.-B. Eom, Y.-H. Jung, D.-W. Lee, B.-S. Kang, "Various design techniques to reduce cogging torque by controlling energy variation in permanent magnet motors", *IEEE Transactions on Magnetics*, vol. 37, no. 4, pp. 2806–2809, 2001, doi:10.1109/20.951313.

[5] C. S. Koh, J.-S. Seol, "New cogging-torque reduction method for brushless permanent-magnet motors", *IEEE Transactions on Magnetics*, vol. 39, no. 6, pp. 3503–3506, 2003, doi:10.1109/TMAG.2003.819473.

[6] T. Li, G. Slemon, "Reduction of cogging torque in permanent magnet motors", *IEEE Transactions on Magnetics*, vol. 24, no. 6, pp. 2901–2903, 1988, doi:10.1109/20.92282.

[7] T. Ishikawa, G. Slemon, "A method of reducing ripple torque in permanent magnet motors without skewing", *IEEE Transactions on Magnetics*, vol. 29, no. 2, pp. 2028–2031, 1993, doi:10.1109/20.250808.

[8] I.-H. Jo, H.-W. Lee, G. Jeong, W.-Y. Ji, C.-B. Park, "A Study on the Reduction of Cogging Torque for the Skew of a Magnetic Geared Synchronous Motor", *IEEE Transactions on Magnetics*, vol. 55, no. 2, pp. 1–5, 2019, doi:10.1109/TMAG.2018.2873310.

[9] F. Scuiller, "Magnet Shape Optimization to Reduce Pulsating Torque for a Five-Phase Permanent-Magnet Low-Speed Machine", *IEEE Transactions on Magnetics*, vol. 50, no. 4, pp. 1–9, 2014, doi:10.1109/TMAG.2013.2287855.

[10] H. Y. Sun, K. Wang, "Effect of Third Harmonic Flux Density on Cogging Torque in Surface-Mounted Permanent Magnet Machines", *IEEE Transactions on Industrial Electronics*, vol. 66, no. 8, pp. 6150–6158, 2019, doi:10.1109/TIE.2018.2875639.

[11] M. Lukaniszyn, M. JagieLa, R. Wrobel, "Optimization of permanent magnet shape for minimum cogging torque using a genetic algorithm", *IEEE Transactions on Magnetics*, vol. 40, no. 2, pp. 1228–1231, 2004, doi:10.1109/TMAG.2004.825185.

[12] P. S. Shin, S. H. Woo, C. S. Koh, "An Optimal Design of Large Scale Permanent Magnet Pole Shape Using Adaptive Response Surface Method With Latin Hypercube Sampling Strategy", *IEEE Transactions on Magnetics*, vol. 45, no. 3, pp. 1214–1217, 2009, doi:10.1109/TMAG.2009.2012565.

[13] R. Lateb, N. Takorabet, F. Meibody-Tabar, "Effect of magnet segmentation on the cogging torque in surface-mounted permanent-magnet motors", *IEEE Transactions on Magnetics*, vol. 42, no. 3, pp. 442–445, 2006, doi:10.1109/TMAG.2005.862756.

[14] M. Ashabani, Y. A.-R. I. Mohamed, "Multiobjective Shape Optimization of Segmented Pole Permanent-Magnet Synchronous Machines With Improved Torque Characteristics", *IEEE Transactions on Magnetics*, vol. 47, no. 4, pp. 795–804, 2011, doi:10.1109/TMAG.2010.2104327.

[15] K. Abbaszadeh, F. Rezaee Alam, S. Saied, "Cogging torque optimization in surface-mounted permanent-magnet motors by using design of experiment", *Energy Conversion and Management*, vol. 52, no. 10, pp. 3075–3082, 2011, doi:https://doi.org/10.1016/j.enconman.2011.04.009, URL: https://www.sciencedirect.com/science/article/pii/S0196890411001397.

[16] S. Chaithongsuk, N. Takorabet, F. Meibody-Tabar, "On the Use of Pulse Width Modulation Method for the Elimination of Flux Density Harmonics in the Air-Gap of Surface PM Motors", *IEEE Transactions on Magnetics*, vol. 45, no. 3, pp. 1736–1739, 2009, doi:10.1109/TMAG.2009.2012801.

[17] S. Chaithongsuk, N. Takorabet, B. Nahid-Mobarakeh, F. Meibody-Tabar, "Optimal design of PM motors for quasi-sinusoidal air-gap flux density", *in 45th International Universities Power Engineering Conference UPEC2010*, pp. 1–6, 2010.

[18] J. A. Houldsworth, D. A. Grant, "The Use of Harmonic Distortion to Increase the Output Voltage of a Three-Phase PWM Inverter", *IEEE Transactions on Industry Applications*, vol. IA-20, no. 5, pp. 1224–1228, 1984, doi:10.1109/TIA.1984.4504587.

[19] IEEE 1812-2014, "IEEE Trial-Use Guide for Testing Permanent Magnet Machines", [Online; accessed 18-September-2019], 2014, URL: https://standards.ieee.org/standard/1812-2014.html.

BIOGRAPHIES

Khristian M. de Andrade Jr received the B.Sc. and M.Sc. degrees in electrical engineering from the Federal University of Goiás, Goiânia, Brazil, where he is currently pursuing the Ph.D. degree.

Bernardo P. de Alvarenga received the B.E. degree from the University of Brasília, Brazil, the M.Sc. degree from the Federal University of Uberlândia, Brazil, and the Ph.D. degree from the University of São Paulo, Brazil, all in electrical engineering. He is currently a Professor with the Federal University of Goiás, Goiânia, Brazil.

Geyverson T. de Paula received the B.E., M.Sc., and Ph.D. degrees in electrical engineering from the University of São Paulo, São Carlos, Brazil. He is currently a Professor with the Federal University of Goiás, Goiânia, Brazil.